Semianalytical Productivity Models for Perforated Completions

Metin Karakas, SPE, and **S.M. Tariq,** SPE, Schlumberger Well Services

SPE 18247

Summary. This paper discusses the effects of various perforation and reservoir parameters on the productivity (or injectivity) of perforated completions. Because of the complex, 3D flow into a spiral system of perforations, productivity analysis of perforated completions is not easily amenable to analytical treatment. This paper presents a semianalytical solution for the estimation of skin in perforated completions. Results are presented for two separate cases: the 2D-plane-flow problem, which is essentially valid at small dimensionless perforation spacings (large perforation penetrations or high perforation shot densities) and the general 3D problem, where the vertical convergent flow into perforations is significant. In these analyses, the wellbore and vertical-flow effects are quantified in terms of pseudoskins obtained by accurate finite-element simulations. The effects of perforation damage and formation anisotropy are also included. The results provide a better understanding of the relative role of various perforation parameters in affecting well productivity. Because they are based on theoretical considerations, the correlations allow reliable estimates of the skin in perforated completions.

New relations are provided for estimating productivity of perforated completions with formation permeability damage. Results indicate the importance of angular phasing, in addition to perforation penetration, in overcoming the effects of formation damage on well productivity.

Introduction

Well productivity (or injectivity) is an important consideration in any reservoir development program. While the near-wellbore heterogeneities and the cleanup flow conditions during perforating strongly influence the final outcome, the selection of proper perforating hardware (perforator and gun type) is essential for optimizing productivity in perforated completions. A theoretical analysis of productivity under idealized reservoir conditions can provide some general guidelines for achieving this objective. Such studies also shed considerable light into the perforation-flow problem. Furthermore, accurate productivity estimates are generally required for flow predictions and for completion evaluation. A comparison of the observed well productivity (or skin from well test) with the expected productivity is a useful check on the completion efficiency.

Although gun perforating has been used widely to control production or injection of fluids in oil and gas reservoirs, the effects of various perforation and reservoir parameters on the productivity of perforated completions are not yet fully understood. Productivity analysis of perforated completions, because of the 3D nature of the flow, is significantly more complex than that of openhole completions. The major difficulty arises from two important considerations: the spiral distribution of the perforations in the vertical direction and the presence of the wellbore, which is a barrier to flow into perforations. This study shows that the wellbore effect, which is generally neglected in the productivity analysis of vertically fractured wells, can be important for perforated completions.

Because an analytical treatment is extremely difficult even with simplifying assumptions, various numerical techniques frequently have been used to study the steady-state flow into perforated completions.[1-5] While they provide useful insight into the productivity problem, numerical models do not readily reveal the functional relationship between various perforation and reservoir parameters. Because the large number of system parameters affecting well productivity can assume values over a wide range, a large number of numerical experiments are required to generalize the dependency of well productivity (or perforation skin) on these parameters. Consequently, the reliability of any empirical correlations for estimating skin in perforated completions can be a serious concern.

In this paper, we first consider the simpler 2D steady-state-flow problem, which is essentially valid at small dimensionless perforation spacings (high perforation densities or large perforation penetrations). Using an accurate 2D finite-element model (FEM), we establish the dependency of perforation skin on the angular perforation phasing, the perforation penetration, and the well radius. The wellbore effect on well productivity is formulated in terms of a wellbore pseudoskin. For the general case of 3D flow, we decouple the convergent flow effects from wellbore effects. The vertical flow effects are quantified in terms of a vertical pseudoskin, which is obtained through 3D finite-element simulations. We later extend these results to include the effects of permeability reduction in the crushed zone and formation anisotropy. Finally, we examine the combined effect of formation damage and perforations on well productivity. As verified, these semianalytical productivity models provide a good estimate of skin in perforated completions for a wide range of perforation parameters.

Background

The effects of perforating parameters on the well flow efficiency are well documented. In Muskat's[6] first analytical treatment of the problem, perforations were represented by mathematical sinks distributed spirally around the wellbore and did not extend into the formation. Later, McDowell and Muskat,[7] using electrolytic tank experiments, reported productivity results for perforations extending beyond the well casing.

Harris[1] first used a finite-difference modeling technique to examine the productivity aspects of perforated completions. He also presented a dimensionless analysis of the problem and provided skin-factor curves as a function of dimensionless parameters. While this analysis provided useful insight into the problem, Harris' results were restricted to wedge-shaped in-plane perforations because of limitations of the finite-difference model.

Klotz *et al.*[2] examined the crushed- and damaged-zone effects using a 2D FEM. Hong[3] extended Harris' model to include the effects of drilling damage and various staggered perforation patterns. He also presented his correlations in two separate nomograms for formations with or without a damaged zone. Hong did not verify these correlations.

Later, Locke[4] applied the FEM to model the full 3D problem of flow into perforations by properly taking into account the actual perforation geometry and the spiral nature of their distributions around the wellbore, which is commonly used in real perforating guns. Locke also presented a nomograph for estimating the skin in perforated completions but did not discuss the development of the nomograph or the verification of results.

Using a similar, but more refined, FEM than Locke's, Tariq[5] examined the non-Darcy flow effects in perforated completions and confirmed Locke's productivity results. Tariq pointed out, however, that Locke's productivity estimates were slightly optimistic, mainly because of insufficient grid size in Locke's FEM. Tariq's model, which is used here for the 3D productivity simulations, is also in close agreement with McDowell and Muskat's[7] electrolytic tank experiments.

Problem Statement

In this work, we assume cylindrical perforations surrounded by a crushed zone of reduced permeability. As **Fig. 1** shows, the perforations are distributed spirally around the wellbore. Angular phasing,

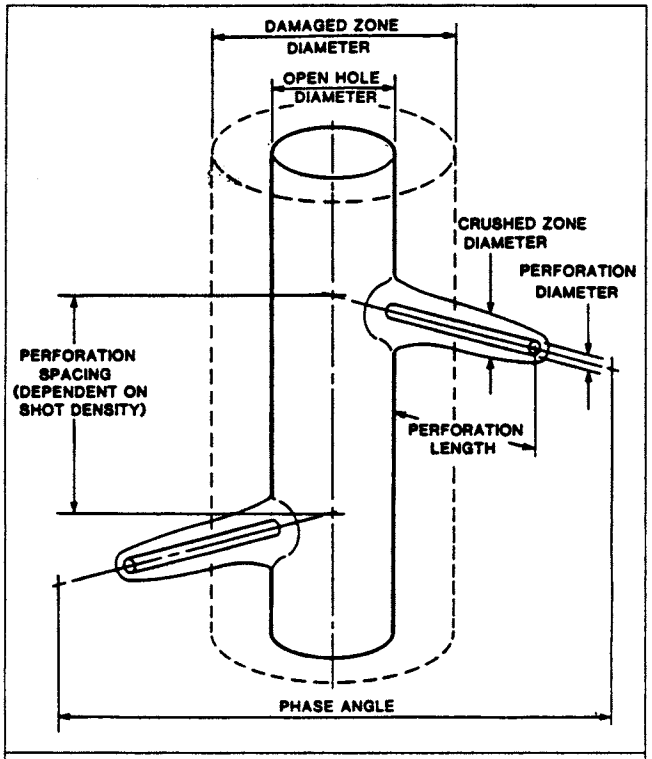

Fig. 1—Perforation geometry.

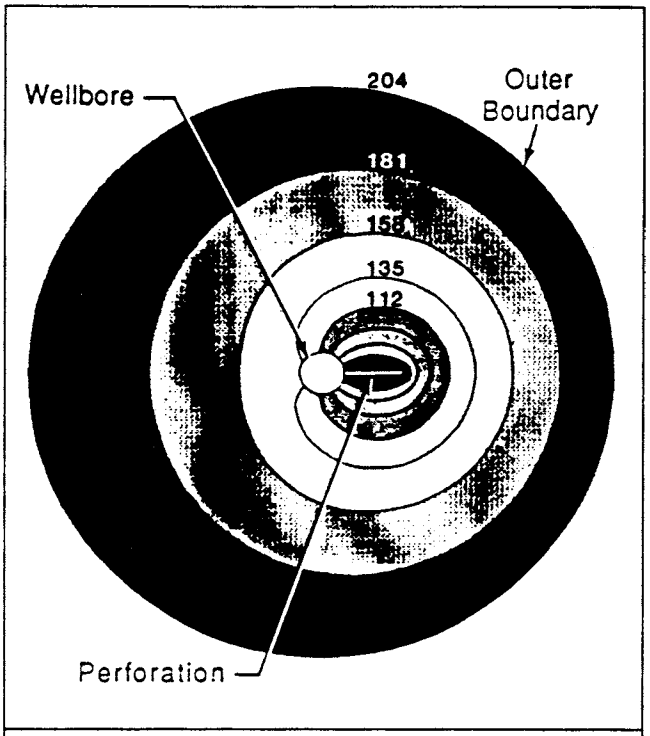

Fig. 2—Pressure distribution around wellbore, 2D simulation, 0° phasing.

θ, denotes the angle between two successive perforations. The perforation or shot density, n_s, refers to number of perforations per foot of formation. It is assumed that perforation spacing, h, is constant and inversely proportional to the perforation density ($h=1/n_s$) and that the formation thickness, h_t, is large enough that no appreciable end effects owing to uneven perforation spacing are present.

The following assumptions are made concerning the porous media and the fluids.

1. The reservoir consists of a single-layer cylindrical formation of constant thickness.
2. The reservoir fluid is single-phase and incompressible.
3. The flow is laminar.
4. The drainage radius of the reservoir, r_e, is significantly larger than the perforation penetration radius ($r_e \gg r_w + L_p$).
5. Anisotropy ratio, k_H/k_V, is constant throughout the reservoir.

The problem with this set of assumptions is reduced to solving the steady-state potential equation with suitable boundary conditions.[1] In this study, we assume constant potentials at the drainage radius, r_e, and at the well. The pressure drops inside the perforations are assumed to be negligible.

The steady-state flow into a perforated well can be described by[1]

$$q_p = \frac{2\pi k h_t (p_e - p_w)}{\mu[\ln(r_e/r_w) + s_t]}. \quad \ldots\ldots\ldots\ldots\ldots\ldots\ldots\ldots\ldots\ldots (1)$$

The total skin factor, s_t, as defined in Eq. 1, is a function of the perforation parameters (e.g., perforation length and diameter) and the formation parameters (e.g., anisotropy and permeability reduction in the formation). Therefore, it includes combined effects of the perforations and any permeability damage in the formation. To differentiate the contribution of the formation damage, the total skin is generally expressed in terms of two separate components[3]:

$$s_t = s_p + s_{dp}. \quad \ldots\ldots\ldots\ldots\ldots\ldots\ldots\ldots\ldots\ldots\ldots\ldots\ldots\ldots (2)$$

The perforation skin factor, s_p, indicates the relative efficiency of a perforated well compared with an ideal openhole completion (geometrical skin in an undamaged formation). On the other hand, the damage skin factor, s_{dp}, provides an estimate of the treatable skin in perforated completions.

Perforation Skin

In formations with no significant formation and perforation damage, the perforation skin, s_p, would be a function of the perforation phase angle, θ; the perforation length, L_p; the perforation radius, r_p; the perforation shot density, n_s (or vertical spacing between perforations, h); and the well radius, r_w. Naturally, the relative importance of these parameters to well productivity depends on the system's dimensionless parameters and can vary significantly. In this work, three dimensionless variables are introduced: dimensionless perforation spacing,

$$h_D = (h/L_p)\sqrt{k_H/k_V}; \quad \ldots\ldots\ldots\ldots\ldots\ldots\ldots\ldots\ldots\ldots (3)$$

dimensionless perforation radius,

$$r_{pD} = (r_p/2h)(1+\sqrt{k_V/k_H}); \quad \ldots\ldots\ldots\ldots\ldots\ldots\ldots\ldots\ldots\ldots (4)$$

and dimensionless well radius,

$$r_{wD} = r_w/(L_p + r_w). \quad \ldots\ldots\ldots\ldots\ldots\ldots\ldots\ldots\ldots\ldots\ldots\ldots (5)$$

As discussed earlier, the general 3D problem is not easily amenable to analytical treatment. A general solution incorporating a numerical model would require mapping s_p in 3D parameter space for various phasings, which, depending on the range of parameters, could be quite laborious because of the complexity of the problem. To obtain a tractable solution, we elected to study first the simpler 2D problem, the solution of which essentially forms the basis for the solution of the full 3D problem. In the 2D analysis, we ignore any vertical flow into perforations. Therefore, the flow into the perforations is considered independent of the vertical coordinate. As shown later, the negligible vertical flow assumption is justified at small dimensionless perforation spacings, h_D (high perforation shot densities or long perforation lengths).

Analysis of the plane flow into perforations (shown in the following sections) is important for two reasons: it can establish a basis for the solution of the general 3D problem (in analogy to full- vs. limited-height vertical hydraulic fracture problems) and gives insight into the relative importance of various perforation parameters on well productivity.

2D Analysis

For most practical perforation lengths and the well radii ($L_p \geq 3$ in. [7.6 cm] and $r_w \leq 10$ in. [25.4 cm]), the perforation diameter

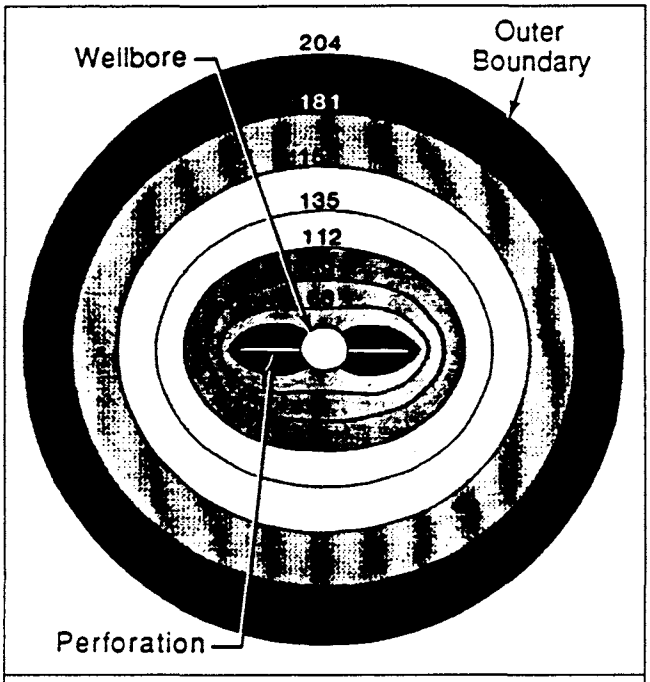

Fig. 3—Pressure distribution around wellbore, 2D simulation, 180° phasing.

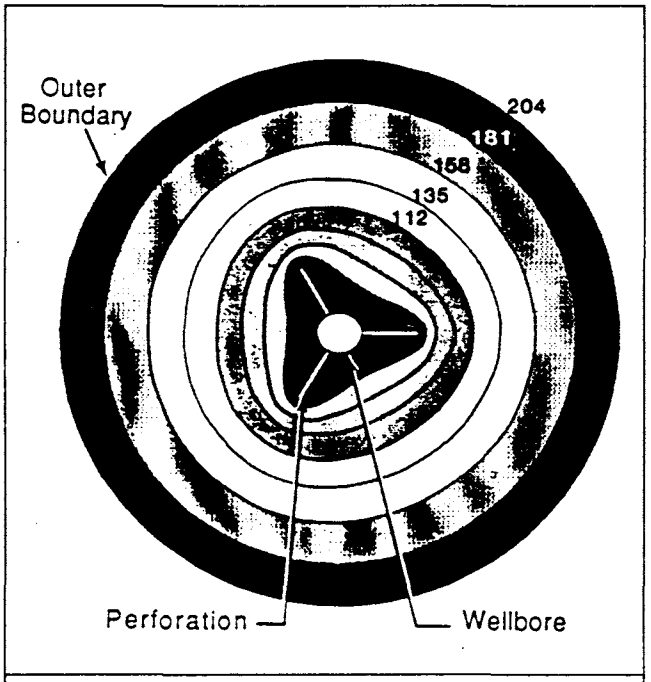

Fig. 4—Pressure distribution around wellbore, 2D simulation, 120° phasing.

(assuming negligible vertical flow) would have minimal effect on well productivity. Therefore, under these conditions, s_p would essentially be controlled by θ, L_p, and r_w. Furthermore, for analysis purposes, the cylindrical perforations can be replaced with a thin strip of length L_p.

Fig. 2 shows the pressure distribution in the reservoir for 0° (or 360°) phasing with $L_p = 10$ in. [25.4 cm] and $r_w = 4.0$ in. [10 cm]. The solution was obtained with ANSYS,[8] a general-purpose commercial finite-element code (see Ref. 9 for a more detailed description of the numerical model). The pressure increase is uniform from the perforation. As Fig. 2 shows, the 2D flow behavior into perforations is quite similar to that of an infinite-conductivity, vertically fractured well. The equipressure lines are close to confocal ellipses with some distortion from the presence of the wellbore. The concentricity point is about mid-perforation length. The flux distribution at perforation, as for a vertical fracture, is significantly higher at the perforation tip and root. Because the wellbore is a complete barrier to reservoir flow, flow efficiency is reduced.

Figs. 3 through 5 show the pressure distribution in the reservoir for 180, 120, and 90° phasings, respectively. For these cases, the perforation and reservoir parameters are identical to the 0°-phasing simulation. For 180° phasings, the equipressure lines are, as expected, confocal ellipses, with less distortion from the wellbore. Moreover, the concentricity point is the center of the well. Consequently, the effective length scale for the well productivity includes perforation length and well radius. As Figs. 4 and 5 show, the pressure distribution in the reservoir for 120 and 90° phasings are more circular than that for 0 and 180° phasings, indicating more efficient flow patterns. Finally, the effective well radius approaches its maximum ($r_w + L_p$) with smaller phasings ($\theta \rightarrow 0°$). Moreover, the wellbore interference with reservoir flow is less significant with smaller phasings because more fluid enters at the perforation tips.

Under plane-flow conditions and assuming negligible wellbore effects (small r_{wD}), the "effective well radius" concept, developed by Prats[10] for vertically fractured wells, can easily be extended to perforated completions:

$$s_p = s_H = \ln\left(\frac{r_w}{r_{we}}\right), \quad \ldots\ldots\ldots\ldots\ldots\ldots\ldots\ldots\ldots\ldots (6)$$

where the pseudoskin, s_H, is used to distinguish the plane-flow effects from the vertical-flow and wellbore effects. The effective well radius, r_{we}, is given by

$$r_{we}(\theta) = \begin{cases} \frac{1}{4}L_p & \text{if } \theta = 0° \\ \alpha_\theta (r_w + L_p) & \text{otherwise} \end{cases} \quad \ldots\ldots\ldots\ldots\ldots\ldots\ldots\ldots (7)$$

Note that the effective penetration for multidirectional perforations ($\theta = 180$, 120, 90°, etc.) includes both perforation penetration and well radius. **Table 1** shows the dependency of the variable α_θ in Eq. 7 on θ for various phasings.

In this study, the numerical values for α_θ were obtained through finite-element simulations for all the phasings except for 0 (or 360) and 180° phasings, for which Prats'[10] vertical fracture solutions are directly applicable. In these simulations, the wellbore effects were minimized by assuming a small value for the dimensionless well radius ($r_{wD} \leq 0.01$).

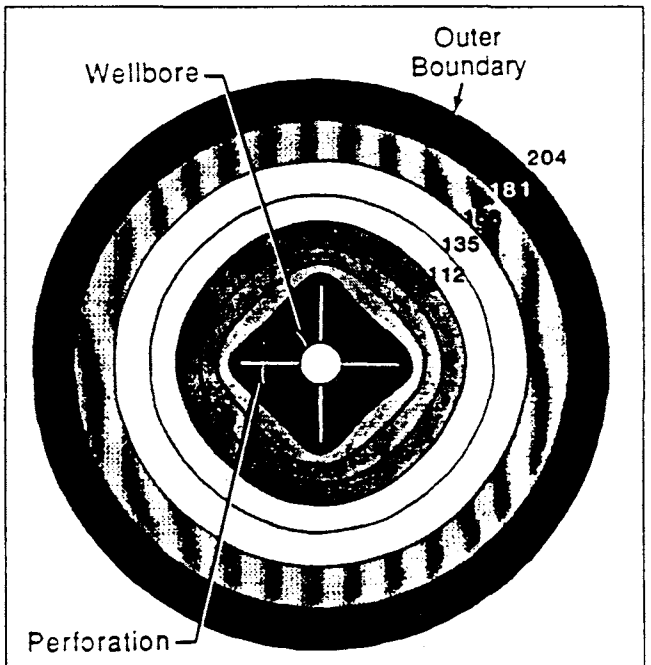

Fig. 5—Pressure distribution around wellbore, 2D simulation, 90° phasing.

TABLE 1—DEPENDENCY OF r_{we} ON PHASING

Perforation Phasing (degrees)	$r_{we}/(r_w+L_p)$
0 (360)	0.250
180	0.500
120	0.648
90	0.726
60	0.813
45	0.860

Wellbore Effects for 2D Flow

As discussed earlier, the wellbore is a complete barrier to the flow into 0°-phased perforations and interferes partially with the flow into multidirectional phasings. Depending on the system's geometric parameters, this wellbore effect can be quite significant for well productivity. As a result of the additional pressure drop, well productivity would be less than that estimated with Eq. 7. Thus, this effect can be quantified in terms of a wellbore pseudoskin, s_{wb}, which is always positive:

$$s_p = s_H + s_{wb}. \quad \text{(8)}$$

The dependency of s_{wb} on r_{wD} can readily be obtained by subtracting s_H as defined in Eq. 6 from the perforation skin obtained through 2D finite-element simulations. **Fig. 6** illustrates this dependency for various phasings. As shown, the wellbore skin for a given dimensionless well radius is significantly larger for 0° phasing than for the multidirectional phasings. Furthermore, the wellbore effect (for $r_{wD} \leq 0.5$) is quite small for phasings smaller than 120°.

The wellbore skin, s_{wb}, can be closely approximated by

$$s_{wb}(\theta) = c_1(\theta)\exp[c_2(\theta)r_{wD}] \quad \text{(9)}$$

for $0.30 \leq r_{wD} \leq 0.90$, where c_1 and c_2 are given in **Table 2** for various phasings.

Discussion of 2D Results

The results of 2D analysis, although strictly valid only when vertical-flow effects are negligible, provide useful insight into the role played by the perforation phasing and length on the productivity of perforated completions.

For the unidirectional (0°-phasing) perforations, productivity increases logarithmically with perforation length. Also, depending on r_{wD}, the wellbore can significantly affect the productivity of 0°-phased perforations, whereas productivity increases with the total formation penetration ($r_w + L_p$) in multidirectional perforations. Therefore, other parameters being equal, changing (or reducing) the phasings from 0 to 180° would more than double the effective perforation penetration. Moreover, wellbore effects are significantly reduced with the multidirectional perforations. At plane-flow conditions (no vertical flow convergence into perforations), well productivity will continue to improve with smaller phasings. Because the effective well radius (as shown in Table 1) logarithmically approaches its maximum value of ($r_w + L_p$), the observed gain in productivity with phasing is less significant at small phasings.

Because the vertical-flow effects are assumed negligible, the 2D results provide an upper bound on the attainable productivity for a given set of perforation parameters. McDowell and Muskat[2] first observed that the productivity of a perforated completion could be

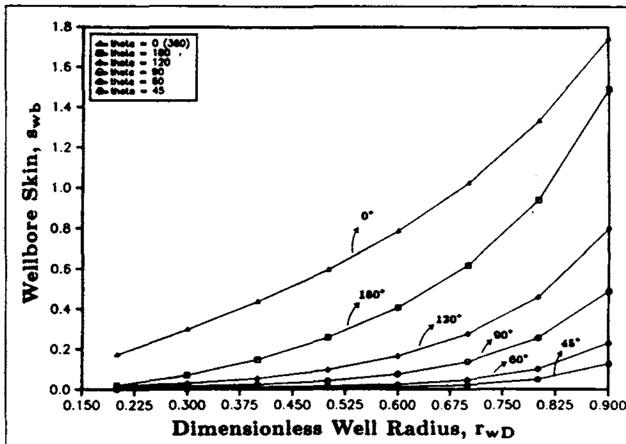

Fig. 6—Wellbore skin as a function of perforation phasing, 2D results.

better than that of an ideal openhole completion of identical well radius. A necessary condition for the minimum perforation length for equal or better productivities can easily be derived for various phasings from Eqs. 6 through 8 and the 2D wellbore-skin correlations. Assuming negligible vertical convergent effects, this condition ($s_p \leq 0$) is satisfied when

$$L_{p\min}(\theta) \geq c_3(\theta)r_w, \quad \text{(10)}$$

where c_3 is given in **Table 3** for various phasings.

As Table 3 shows, the minimum penetration requirement for equivalent openhole productivities is significantly larger for unidirectional 0° phasing than for multidirectional phasings.

Vertical-Flow Effects

In the preceding analysis, the vertical converging flow effects into perforations were completely ignored. As mentioned, the condition for this assumption (for most practical ranges of perforation lengths) rests largely on the premise of small dimensionless perforation spacing. The vertical convergent flow into perforations, in analogy to the horizontal-well problem,[11-13] causes additional pressure drop and therefore adversely affects well productivity. **Fig. 7** compares the perforation skin obtained by 3D finite-element simulations and by the 2D skin equations (Eqs. 6 and 7) for 0° phasing. To minimize any wellbore effects, a relatively small well (r_w=0.5 in. [1.3 cm]) was used. The perforation skin is shown as a function of h_D and r_{pD}. As this plot shows, at large h_D (low shot densities) the actual perforation skin is significantly higher than that predicted by the plane-flow considerations alone.

The additional pressure drop caused by the vertical converging flow into perforations can thus be quantified in terms of a vertical pseudoskin, s_V. Assuming a small dimensionless well radius, the perforation skin would therefore be given by

$$s_p \simeq s_H + s_V. \quad \text{(11)}$$

The dependency of s_V on h_D and r_{pD} can be obtained by subtracting the horizontal skin contribution (Eq. 6), s_H, from the perforation skin, s_p (Eq. 11), obtained through 3D finite-element simulations.

TABLE 2—VARIABLES c_1 AND c_2 IN EQ. 9

Perforation Phasing (degrees)	c_1	c_2
0 (360)	1.6×10^{-1}	2.675
180	2.6×10^{-2}	4.532
120	6.6×10^{-3}	5.320
90	1.9×10^{-3}	6.155
60	3.0×10^{-4}	7.509
45	4.6×10^{-5}	8.791

TABLE 3—MINIMUM PERFORATION LENGTH FOR $s_p \leq 0$ AS A FUNCTION OF PHASING

Perforation Phasing (degrees)	$L_{p\min}/r_w$
0 (360)	4.62
180	1.37
120	0.77
90	0.53
60	0.33
45	0.23

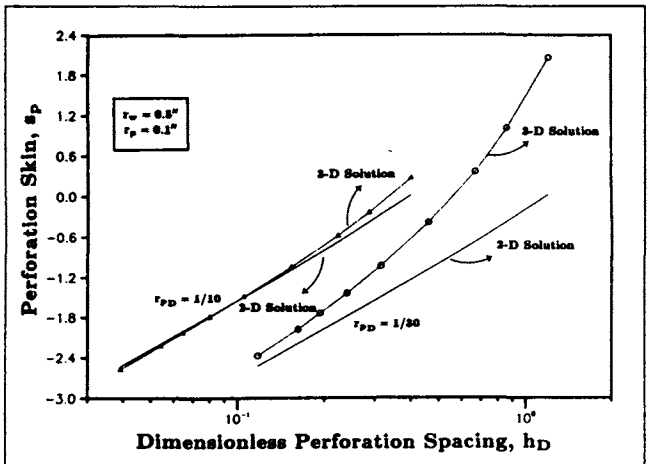

Fig. 7—Comparison of 3D and 2D solutions, 0° phasing.

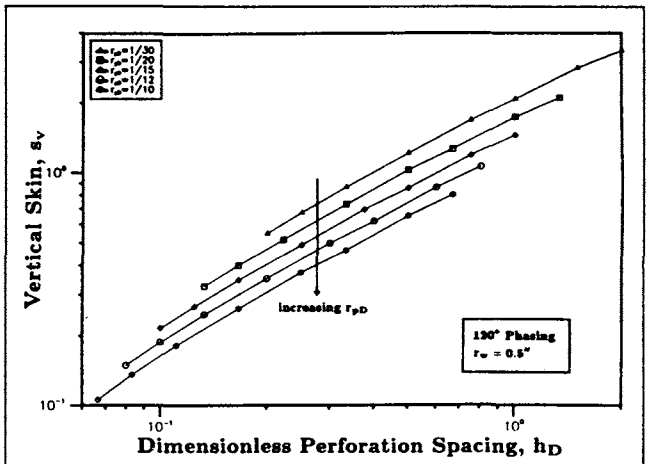

Fig. 8—Vertical-skin correlations, 120° phasing.

Fig. 8 gives the vertical skin correlations for 120° phasing. In 3D simulations, the dimensionless well radius was kept small to minimize any wellbore effects. As expected, the vertical resistance to flow, s_V, increases with the dimensionless perforation spacing (low perforation shot densities), h_D, and decreases with the dimensionless perforation radius, r_{pD} (increasing surface area for vertical flow).

The vertical pseudoskin factors can be approximated well for various phasings by

$$s_V = 10^a h_D^{b-1} r_{pD}^{b}, \quad \ldots\ldots\ldots\ldots\ldots\ldots\ldots\ldots\ldots\ldots (12)$$

where $a = a_1 \log_{10} r_{pD} + a_2$ ..... (13)

and $b = b_1 r_{pD} + b_2$. ..... (14)

Table 4 lists the values of a_1, a_2, b_1, and b_2. As shown later, these equations can be used to estimate the perforation skin factor for most practical ranges of system parameters ($h_D \le 10$ and $r_{pD} \ge 0.01$).

Fig. 9 illustrates the effect of phasing on vertical skin. For a given perforation penetration and radius, s_V increases with decreasing phasing angle between perforations, as seen in Fig. 9. This dependency of s_V on θ results from the spiral distribution of perforations around the wellbore, which introduces a chaotic vertical converging flow pattern into perforations. Other parameters being equal, this increase in vertical resistance with phasing is more pronounced at small dimensionless perforation spacings (low shot densities). It is expected that, because of the orderly vertical convergence, the vertical skin would be significantly smaller in in-plane perforations. Because of other considerations (reservoir heterogeneities, casing strength, etc.), however, spiral perforations are usually preferred over in-plane perforations.

Because of the dependency of s_V on θ, the productivity gain observed at small h_D (high shot densities) through phasing can be partially or totally offset by increases in the vertical resistance to flow at high h_D (low shot densities). The net effect therefore depends on the particular values of the system parameters. From a theoretical viewpoint, the "optimum phasing" for a given set of perforation and reservoir parameters would essentially be controlled by the perforation shot density. For most practical ranges of perforation and reservoir parameters, however, productivity improves significantly with smaller angular phasings.

At small dimensionless well radii, the vertical flow into 0°-phased perforations extending from a relatively small well is analogous to the horizontal-well problem. Therefore, vertical-skin solutions developed for horizontal wells[11-13] for practical ranges of h_D and r_{pD} would be equally applicable for 0°-phased perforations. An approximate relation for s_V when $h_D \le 5$ can be inferred from Kuchuk *et al.*'s[13] work:

$$s_V = -h_D \ln(2\pi r_{pD}) - (1/12) h_D^2. \quad \ldots\ldots\ldots\ldots\ldots\ldots\ldots\ldots\ldots\ldots (15)$$

Fig. 10 compares the numerically derived vertical-skin correlations with those obtained from Eq. 15. In general, the comparison between the two solutions is satisfactory, except at large values of r_{pD}. Nevertheless, the vertical skin is relatively small for these ranges of perforation parameters and would minimally affect well productivity.

In general, Eq. 15 provides useful information on the nature of the dependency of vertical skin on perforation parameters. The vertical skin essentially increases linearly with h_D but decreases logarithmically with r_{pD}. This dependency has been observed in our vertical-skin correlations for all the phasings and for the ranges of dimensionless parameters considered. As observed from Eq. 15, the relative importance of perforation parameters in minimizing the vertical skin varies depending on the actual values of the dimensionless parameters. From the overall productivity viewpoint, however, the importance of deep perforation penetrations, as commonly recognized in the industry, is quite evident.

TABLE 4—VERTICAL-SKIN CORRELATION COEFFICIENTS

Perforation Phasing (degrees)	a_1	a_2	b_1	b_2
0 (360)	−2.091	0.0453	5.1313	1.8672
180	−2.025	0.0943	3.0373	1.8115
120	−2.018	0.0634	1.6136	1.7770
90	−1.905	0.1038	1.5674	1.6935
60	−1.898	0.1023	1.3654	1.6490
45	−1.788	0.2398	1.1915	1.6392

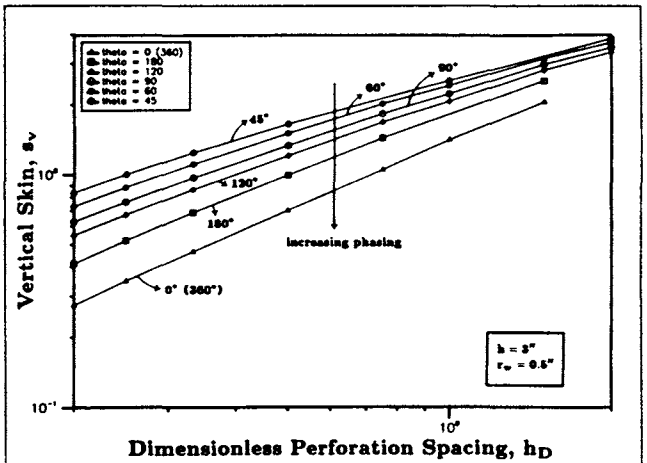

Fig. 9—Effect of phasing on vertical flow.

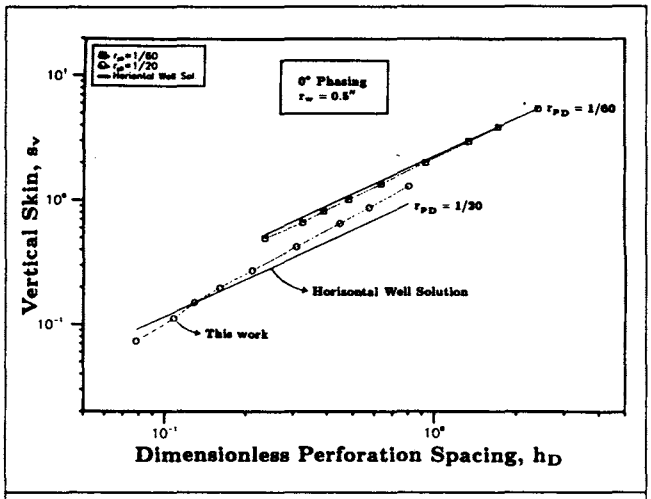

Fig. 10—Comparison of vertical-skin correlations with horizontal-well solutions.

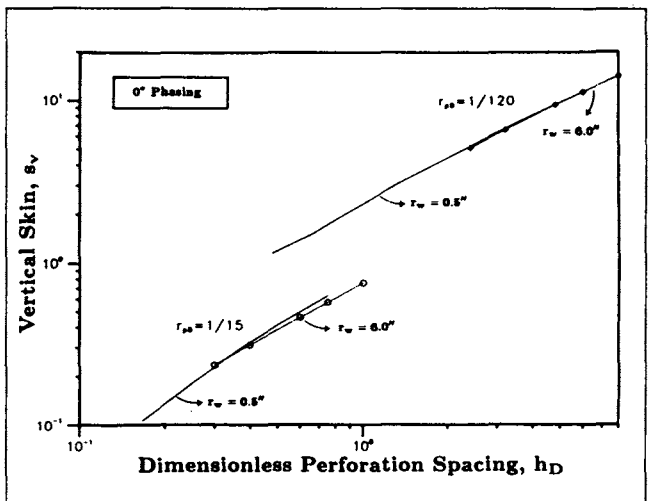

Fig. 11—Wellbore effect, 3D simulation, 0° phasing.

Wellbore Effects for 3D Flow

In the previous analysis, it was assumed that the wellbore had no appreciable effect on the vertical converging flow. It is expected that the wellbore would significantly affect the flow into perforations at large dimensionless well radii and large dimensionless perforation spacings. As **Fig. 11** shows, however, the vertical-skin correlations for a large wellbore (r_w=6 in. [15 cm]) closely follow those obtained with a relatively small wellbore (r_w=0.5 in. [1.3 cm]) when the vertical-skin estimates are corrected for wellbore effects with the 2D wellbore-skin correlations. Consequently, it can be assumed that the major wellbore effect can be accounted for by plane-flow considerations alone for the practical ranges of perforation parameters:

$$s_p = s_H + s_V + s_{wb}, \quad \ldots\ldots\ldots\ldots\ldots\ldots\ldots\ldots\ldots\ldots (16)$$

where s_{wb} is obtained with 2D wellbore-skin correlations.

Crushed-Zone Effects

As discussed extensively in the literature,[2,4,14] permeability damage around the perforations from rock compaction can significantly impair well productivity. In terms of reservoir flow, the major effect of a crushed (compacted) zone is to induce additional resistance to vertical flow into perforations (radially converging vertical flow). The effect of a crushed zone at plane-flow conditions would be quite negligible (linear flow into perforations). An analogous situation would be a vertical fracture with skin. As Prats[10] showed, this skin effect is usually small for fractured wells. Assuming radial flow around the perforations in the vertical plane and negligible wellbore effects, the additional pressure drop caused by the crushed zone, in analogy to mechanical skin formulation in vertical wells, could be taken into account by

$$s_c = \frac{h}{L_p}\left(\frac{k}{k_c} - 1\right)\ln\left(\frac{r_c}{r_p}\right). \quad \ldots\ldots\ldots\ldots\ldots\ldots\ldots\ldots\ldots\ldots (17)$$

McLeod's[14] similar expression for crushed-zone skin, s_c, is applicable only to formations with no drilling damage. Strictly speaking, Eq. 17 can be used for situations with negligible wellbore effects. As shown with large sets of simulations, however, this formulation generally provides a good approximation to the crushed-zone problem.

Anisotropy Effects

As Muskat[6] pointed out and Tariq[8] later showed, the relative productivity of perforated completions decreases with an increase in the k_H/k_V ratio. Obviously, the vertical skin increases significantly in anisotropic reservoirs where $k_H > k_V$. As Muskat discussed, the solutions for isotropic formations can also be used for anisotropic formations, provided that the dimensionless height and perforation radius are properly modified. In anisotropic formations, the dimensionless spacing is modified by the square root of the anisotropy ratio. In addition, the flow into perforations in the vertical plane is elliptical in anisotropic formations. Therefore, the effective equivalent perforation radius in an anisotropic formation is given by[15,16]

$$r_{pe} = (r_p/2)(1+\sqrt{k_V/k_H}). \quad \ldots\ldots\ldots\ldots\ldots\ldots\ldots\ldots\ldots\ldots (18)$$

Damaged-Zone Effects

Formation damage caused by filtrate invasion during drilling can significantly reduce the productivity of openhole completions. In terms of reservoir flow, the formation damage can be modeled as a finite region of reduced permeability around the wellbore. For an openhole completion, the additional pressure drop caused by the damaged zone can be formulated in terms of a damaged-zone skin factor[8]:

$$s_{do} = [(k/k_d) - 1]\ln(r_d/r_w). \quad \ldots\ldots\ldots\ldots\ldots\ldots\ldots\ldots\ldots\ldots (19)$$

The damaged-zone effect on the productivity of perforated completions is significantly more complex than suggested by Eq. 19. A common mistake made in calculating the total skin in perforated completions is to combine the perforation skin, s_p, with the openhole damage skin, s_{do}.[14]

As Klotz *et al.*[2] and Hong[3] pointed out, the contribution of the damaged zone to total skin in perforated completions depends largely on the relative position of the perforations with respect to the damaged-zone radius. As shown in the Appendix, the damage skin for perforations terminating inside the damaged zone can be approximated by

$$s_{dp} = \left(\frac{k}{k_d} - 1\right)\left[\ln\left(\frac{r_d}{r_w}\right) + s_p\right] + \frac{k}{k_d}s_x, \quad \ldots\ldots\ldots\ldots\ldots\ldots (20)$$

where s_x=pseudoskin to account for boundary effects for perforations terminating close to the damaged-zone boundary. As shown in the Appendix, s_x generally is negligible for $r_d \geq 1.5(r_w + L_p)$. Combining Eqs. 2 and 20 results in

$$s_t = s_{do} + (k/k_d)(s_p + s_x). \quad \ldots\ldots\ldots\ldots\ldots\ldots\ldots\ldots\ldots\ldots (21)$$

This relationship provides the basis for combining s_{do} and s_p to arrive at the total skin for perforations terminating inside the damaged zone.

The implications of Eq. 20 or 21 are quite significant for the productivity of perforated completions where perforations terminate inside the damaged zone. For inefficient perforations ($s_p > 0$), s_{do} is augmented by the product of s_p and the ratio of formation permeability to damaged-zone permeability, k/k_d, which can severely reduce the well productivity. On the other hand, s_{do} is reduced by

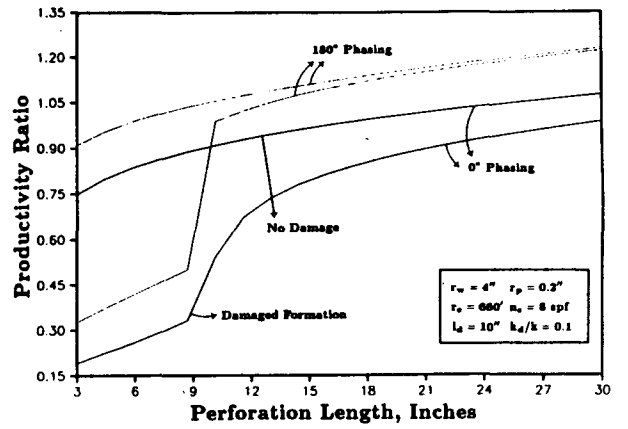

Fig. 12—Effect of phasing on damaged formations.

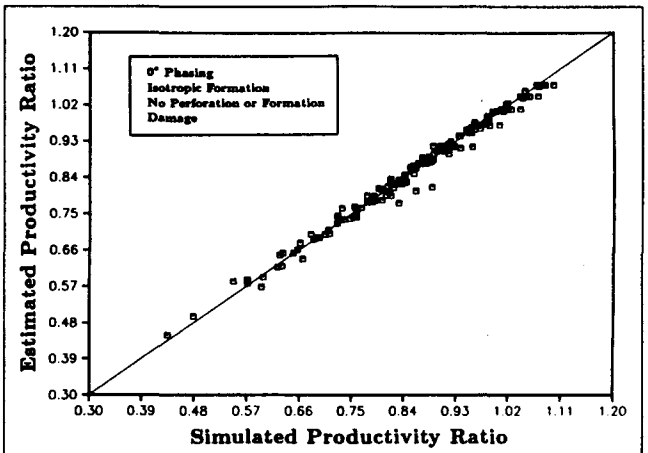

Fig. 13—Comparison with data bank, 0° phasing.

the same product for efficient perforations ($s_p < 0$). As can be observed from the definition of horizontal skin factor, the total skin in damaged formations is always positive for perforations terminating inside the damaged zone.

The flow behavior into perforations significantly changes for perforations extending beyond the damaged zone. For highly damaged formations ($k_d = 0$), the effective perforation length is reduced to the penetration outside the damaged zone ($L_p - L_d$). At the same time, the well radius effectively increases to r_d. For formations with a finite permeability in the damaged zone, the well radius and the perforation length can be modified by

$$L_p' = L_p - [1 - (k_d/k)]L_d \quad \ldots\ldots\ldots\ldots\ldots\ldots\ldots\ldots\ldots\ldots (22)$$

and $$r_w' = r_w + [1 - (k_d/k)]L_d. \quad \ldots\ldots\ldots\ldots\ldots\ldots\ldots\ldots\ldots\ldots (23)$$

Thus, the total skin would correspond to the perforation skin, s_p, obtained with the modified perforation length, L_p', and modified well radius, r_w'. The relations provided by Eqs. 22 and 23 are based on heuristic grounds and are strictly valid for the two limiting conditions ($k_d = 0$ and $k_d = k$). Numerical experiments have verified, however, that these relations provide good estimates of the skin for perforations penetrating beyond the damaged zone.

The analysis provided above for perforations extending beyond the damaged zone indicates that the effect of permeability damage on well productivity is equivalent to the effect of a larger wellbore with reduced perforation penetration into an undamaged formation. Because the total penetration is constant ($r_w + L_p = r_w' + L_p'$), the wellbore skin would be larger than that observed in undamaged formations. Therefore, the effect of formation damage depends largely on the magnitude of r_{wD} at r_w'. As discussed earlier, the wellbore skin for 0°-phased perforations could be substantially higher than that for multidirectional perforations. Therefore, formation damage generally could affect the 0°-phased perforations more significantly. Consequently, the damaged-zone effects can be overcome more easily with the multidirectional perforations. This effect of phasing is illustrated in **Fig. 12**. The effect of drilling damage, s_{dp}, on the 180°-phased perforations can be reduced significantly once the perforations extend beyond the damaged zone. For similar skins, however, substantially deeper penetrations are required for the 0° perforations. In this analysis, equal perforation penetrations are assumed in all directions. For small through-tubing guns, unequal perforation penetrations in various directions would pose a different problem for well productivity and require a separate treatment.

Verification of Correlations

The semianalytical productivity models introduced in this work were verified by comparing their outcome with those obtained through actual, finite-element simulations. For this purpose, an extensive data bank was generated (using FEM to represent various combinations of perforation parameters). Ref. 9 presents further details of the FEM and the data bank used in the verification of the semianalytical correlations and numerical results.

The skin estimates are obtained from various skin formulations introduced in this paper (s_H, s_V, s_{wb}, s_c, and s_{dp}). In the comparisons in **Figs. 13 through 17**, we used the analytical expressions provided in this paper, except for wellbore skin, which was obtained through a simple table-lookup procedure. Because the skin factors vary over a wide range and can be negative, the comparisons are shown in terms of the productivity ratio:

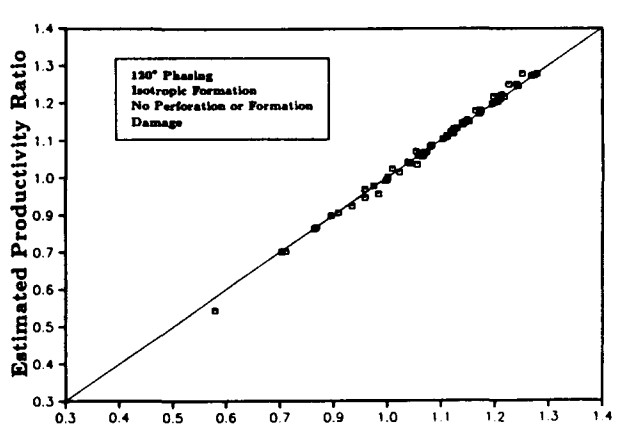

Fig. 14—Comparison with data bank, 120° phasing.

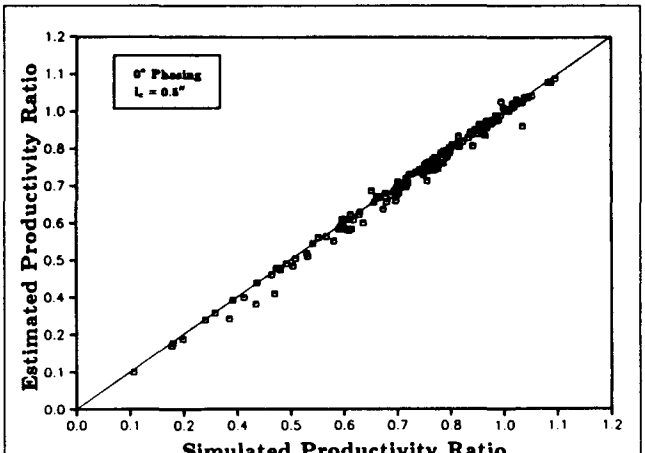

Fig. 15—Comparison with data bank, crushed-zone effects, 0° phasing.

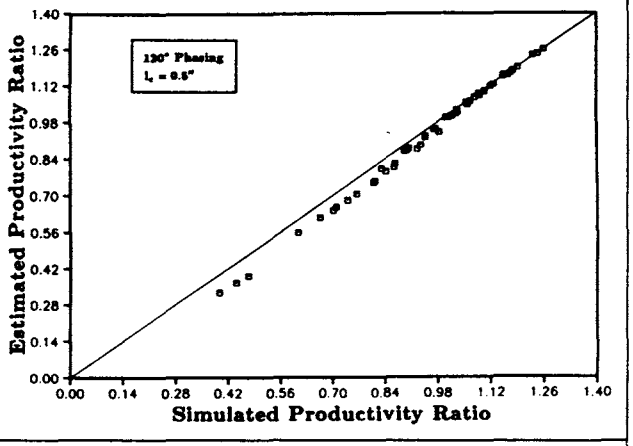

Fig. 16—Comparison with data bank, crushed-zone effects, 120° phasing.

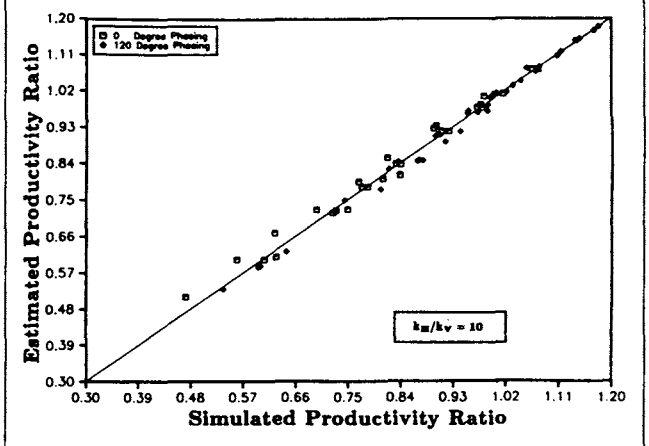

Fig. 17—Comparison with data bank, anisotropic formation.

$$F_p=\frac{q_p}{q_o}=\frac{\ln(r_e/r_w)}{\ln(r_e/r_w)+s_t} \quad \ldots\ldots\ldots\ldots\ldots\ldots\ldots\ldots\ldots\ldots (24)$$

Figs. 13 and 14 show the results for 0 and 120°-phased perforations in an isotropic, undamaged formation, respectively. The predicted values compare quite well with the simulated productivity ratios.

Figs. 15 and 16 compare the correlations for perforations with crushed-zone effects for 0 and 120° phasings, respectively. The crushed-zone skin formulation given by Eq. 17 generally provides good approximation to crushed-zone effects. Fig. 17 shows the comparison for anisotropy ratios of 10 and for 0 and 120° phasings. In these anisotropic simulations, the crushed-zone effects are not included. Figs. 13 through 17 indicate that the skin models introduced in this work provide consistent, reliable estimates of skin in perforated completions for normal ranges of perforation parameters.

Summary of Equations and Procedure for Productivity Evaluation

The theory presented in this paper leads to a simple, systematic, and accurate approach involving the use of algebraic expressions for approximation of skin in a perforated completion. Outlined below is a summary of these equations and a step-by-step procedure for evaluation of skin in a perforated completion:

1. Compute horizontal component of skin, s_H:

$$s_H=\ln(r_w/r_{we}). \quad \ldots\ldots\ldots\ldots\ldots\ldots\ldots\ldots\ldots\ldots (6)$$

The effective well radius, r_{we}, is given by

$$r_{we}(\theta)=\begin{cases} \frac{1}{4}L_p & \text{if } \theta=0° \\ \alpha_\theta(r_w+L_p) & \text{otherwise} \end{cases} \quad \ldots\ldots\ldots\ldots\ldots\ldots (7)$$

The parameter α_θ is given by Table 1.

2. Compute wellbore skin, s_{wb}:

$$s_{wb}(\theta)=c_1(\theta)\exp[c_2(\theta)r_{wD}], \quad \ldots\ldots\ldots\ldots\ldots\ldots\ldots (9)$$

where $r_{wD}=r_w/(L_p+r_w)$. Eq. 9 is valid for $0.30\le r_{wD}\le 0.90$, and c_1 and c_2 are given in Table 2 for various phase angles.

TABLE 5—SKIN CAUSED BY BOUNDARY EFFECT, 180° PHASING

$r_e/(r_w+L_p)$	s_x
18.0	0.000
10.0	−0.001
2.0	−0.002
1.5	−0.024
1.2	−0.085

3. Compute vertical skin, s_V:

$$s_V=10^a h_D^{\,b-1} r_{pD}^{\,b}, \quad \ldots\ldots\ldots\ldots\ldots\ldots\ldots\ldots (12)$$

where $a=a_1 \log_{10} r_{pD}+a_2$ $\ldots\ldots\ldots\ldots\ldots\ldots\ldots\ldots (13)$

and $b=b_1 r_{pD}+b_2$. $\ldots\ldots\ldots\ldots\ldots\ldots\ldots\ldots\ldots\ldots (14)$

The values of a_1, a_2, b_1, and b_2 are given in Table 4. Also,

$$h_D=(h/L_p)\sqrt{k_H/k_V}$$

and $r_{pD}=(r_p/2h)(1+\sqrt{k_V/k_H})$.

Eq. 12 is valid for $h_D\le 10$ and $r_{pD}\ge 0.01$.

4. Determine the combined skin effect caused by perforations, s_p:

$$s_p=s_H+s_V+s_{wb}. \quad \ldots\ldots\ldots\ldots\ldots\ldots\ldots\ldots\ldots\ldots (16)$$

5. Add crushed-zone effects:

$$s_c=\frac{h}{L_p}\left(\frac{k}{k_c}-1\right)\ln\left(\frac{r_c}{r_p}\right), \quad \ldots\ldots\ldots\ldots\ldots\ldots\ldots\ldots (17)$$

$$s_p'=s_p+s_c.$$

6. Add damaged-zone effects. For perforations within damaged zone, the skin caused by the combined effects of perforations and damage is

$$s_t=\left(\frac{k}{k_d}-1\right)\ln\left(\frac{r_d}{r_w}\right)+\left(\frac{k}{k_d}\right)(s_p+s_x),$$

where s_x (given in **Table 5**) is negligible for $r_d\ge 1.5(r_w+L_p)$. For perforations extending beyond the damaged zone, modify the well radius and the perforation length:

$$L_p'=L_p-[1-(k_d/k)]L_d \quad \ldots\ldots\ldots\ldots\ldots\ldots\ldots\ldots (22)$$

and $r_w'=r_w+[1-(k_d/k)]L_d$. $\ldots\ldots\ldots\ldots\ldots\ldots\ldots\ldots (23)$

Use these values in place of L_p and r_w in Steps 1 through 5. The skin value calculated in Step 5 will reflect combined effects of both perforation geometry and damage zone.

7. For anisotropic effects, modify perforation radius, r_p:

$$r_{pe}=(r_p/2)(1+\sqrt{k_V/k_H}), \quad \ldots\ldots\ldots\ldots\ldots\ldots\ldots\ldots (18)$$

and use this value in place of r_p in Steps 1 through 5.

Conclusions

This work presents a theoretical analysis of the productivity of perforated completions. The basic dimensionless groups that control the flow into perforations are identified and their effects on the well productivity shown. Although some results are strictly valid for

idealized reservoir conditions, useful insight is gained for the perforation-flow problem.

At plane-flow conditions (negligible vertical flow), the productivity of perforated completions is essentially governed by the perforation penetration and phasing. In terms of well productivity, the multidirectional perforations (θ=180, 120, and 90°, etc.) offer significant advantages over unidirectional (0°) perforations. In this work, we provide simple, yet accurate, expressions for estimating the relative effects of these parameters for a wide range of perforation parameters.

We have shown that, for most practical ranges of perforation parameters, the effect of converging vertical flow into perforations can be quantified in terms of a vertical pseudoskin, which is a function of the dimensionless perforation spacing, h_D, and radius, r_{pD}. The numerically obtained vertical-skin correlations and the analytical expressions inferred from analogous horizontal-well solutions indicate that the converging vertical-flow effects depend largely on h_D and can be minimized with deep-penetrating perforators and/or high-shot-density perforating guns. Because of the spiral nature of their distributions, the vertical skin increases with smaller phase angles between perforations. Therefore, productivity improvements observed at plane-flow conditions (high perforation shot densities or deep perforation penetrations) through phasing can be partially or totally offset by corresponding increases in vertical skin at high dimensionless perforation spacings (low perforation shot densities).

The crushed zone around perforations essentially increases the vertical resistance to flow. These effects can also be quantified in terms of an additional vertical skin. Consequently, the productivity impairment from a crushed zone can be minimized through deep perforation penetrations or high perforation shot densities.

New relationships are provided for combining openhole damage skin with perforation skin for perforations terminating inside the damaged region. The flow efficiency is quite important for perforations completely terminating inside the damaged zone. The effect of formation damage on the productivity of perforations extending beyond the damaged region is equivalent to the effect of an enlarged wellbore with reduced perforation penetration. Because of the smaller wellbore effects, the formation damage can be overcome more easily with multidirectional phasings.

The productivity correlations are verified extensively with a large set of simulated productivity data. The semianalytical productivity models therefore provide reliable estimates of skin in perforated completions.

Nomenclature

F_p = perforated to ideal openhole productivity ratio
h = spacing between perforations
h_t = total formation thickness
k = formation permeability
k_c = crushed-zone permeability
k_d = damaged-formation permeability
k_H = horizontal permeability
k_V = vertical permeability
L_c = crushed-zone length
L_d = damaged-zone length
L_p = perforation length
L_p' = modified perforation length in damaged formations
n_s = perforation shot density
p_e = pressure at external boundary
p_w = pressure inside wellbore
Δp_t = total steady-state potential pressure drop
Δp_1 = steady-state potential pressure drop in damaged zone
Δp_2 = steady-state potential pressure drop in undamaged zone
q_o = production rate from ideal openhole completion
q_p = production rate from perforated completion
r_c = crushed-zone radius
r_d = damaged-zone radius
r_e = well drainage radius
r_p = perforation radius
r_{pe} = effective perforation radius in anisotropic formations
r_w = well radius
r_w' = modified well radius in damaged formations
r_{we} = effective well radius for perforated completions
s_c = crushed-zone skin
s_{do} = damage skin in openhole completions
s_{dp} = damage skin in perforated completions
s_H = horizontal skin
s_p = perforation skin
s_p' = modified perforation skin
s_t = total skin
s_V = vertical skin
s_{wb} = wellbore skin
s_x = boundary skin
α = variable defined in Eq. 7
θ = angle between successive perforations
μ = viscosity

Subscripts

a = simulated skin
D = dimensionless
e = estimated
min = minimum perforation penetration

Acknowledgments

We thank Piyush C. Shah for stimulating discussions and Schlumberger Well Services Management for permission to publish this paper.

References

1. Harris, M.H.: "The Effect of Perforating on Well Productivity," *JPT* (April 1966) 518-28; *Trans.*, AIME, **237**.
2. Klotz, J.A., Krueger, R.F., and Pye, D.S.: "Effect of Perforation Damage on Well Productivity," *JPT* (Nov. 1974) 1033-44; *Trans.*, AIME, **257**.
3. Hong, K.C.: "Productivity of Perforated Completions in Formations With or Without Damage," *JPT* (Aug. 1975) 1027-38; *Trans.*, AIME, **259**.
4. Locke, S.: "An Advanced Method for Predicting the Productivity Ratio of a Perforated Well," *JPT* (Dec. 1981) 2481-88.
5. Tariq, S.M.: "Evaluation of Flow Characteristics of Perforations Including Nonlinear Effects With the Finite-Element Method," *SPEPE* (May 1987) 104-12.
6. Muskat, M.: "The Effect of Casing Perforations on Well Productivity," *Trans.*, AIME (1943) **151**, 175-87.
7. McDowell, J.M. and Muskat, M.: "The Effect on Well Productivity of Formation Penetration Beyond Perforated Casing," *Trans.*, AIME (1950) **189**, 309-12.
8. Tariq, S.M., Ichara, M.J., and Ayestaran, L.: "Performance of Perforated Completions in the Presence of Anisotropy, Lamination, or Natural Fractures," *SPEPE* (Nov. 1989) 376-84.
9. Karakas, M. and Tariq, S.M.: "Supplement to SPE 18247, Semianalytical Productivity Models for Perforated Completions," paper SPE 21477 available from SPE Book Order Dept., Richardson, TX.
10. Prats, M.: "Effect of Vertical Fractures on Reservoir Behavior—Incompressible Fluid Case," *SPEJ* (June 1961) 105-17; *Trans.*, AIME, **222**.
11. Daviau, G.M. and Bourdarot, G.: "Pressure Analysis for Horizontal Wells," *SPEFE* (Dec. 1988) 716-24.
12. Goode, P.A. and Thambynayagam, R.K.M.: "Pressure Drawdown and Buildup Analysis of Horizontal Wells in Anisotropic Media," *SPEFE* (Dec. 1987) 683-97.
13. Kuchuk, F.J. *et al.*: "Pressure-Transient Behavior for Horizontal Wells With Gas Cap or Aquifer," paper SPE 17413 presented at the 1988 SPE California Regional Meeting, Long Beach, March 23-25.
14. McLeod, O.H. Jr.: "The Effect of Perforating Conditions on Well Performance," *JPT* (Jan. 1983) 31-39.
15. Muskat, M.: *Flow of Homogeneous Fluids*, first edition, McGraw-Hill Book Co. Inc., New York City (1949).
16. Kuchuk, F. and Brigham, W.E.: "Transient Flow in Elliptical Systems," *SPEJ* (Dec. 1979) 401-10; *Trans.*, AIME, **267**.

Appendix—Approximation of Skin for Perforations Within a Damaged Zone

In the following analysis, we assume two concentric annular regions of permeabilities k_d and k. As **Fig. A-1** shows, perforations terminate inside the damaged zone. Furthermore, we assume radial flow in Region 2 with no vertical flow effects.

Authors

Karakas

Tariq

Metin Karakas, an interpretation development engineer, joined Schlumberger-Doll Research in 1981, working on reservoir modeling. Since 1983, he has worked for Schlumberger Well Services on well-test interpretation and reservoir modeling and currently is at the Schlumberger Perforating and Testing Center. He holds a BS degree in chemical engineering from the Middle East Technical U. and an MS degree in petroleum engineering from the U. of Southern California. **Syed M. Tariq** is currently section head of interpretation studies at the Schlumberger Perforating and Testing Center in Rosharon, TX. His current interests focus on evaluation of perforated-well completions, development of completion systems for better productivity, and application of wireline measurements for better completion design. He was a member of the 1986–89 Annual Meeting Program Committee, has been a member of the Editorial Review Committee since 1986, and is 1990 chairman of the General Meeting Committee of the Gulf Coast Section. Tariq holds a BS degree in mechanical engineering from the U. of Karachi and MS and PhD degrees in petroleum engineering from Stanford U.

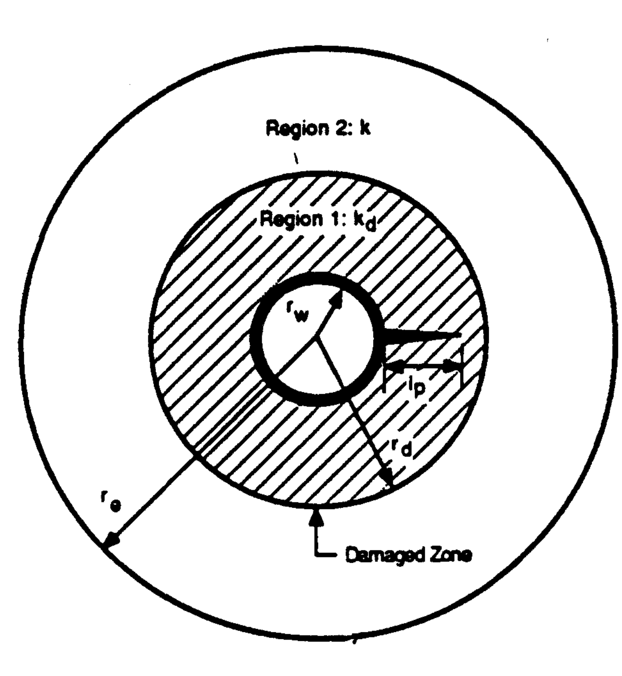

Fig. A-1—Horizontal section of a perforated well with formation damage.

TABLE A-1—DAMAGE SKIN ESTIMATES FOR PERFORATIONS TERMINATING INSIDE THE DAMAGED ZONE, 0° PHASING

		$k_d/k=0.50$		$k_d/k=0.10$		$k_d/k=0.05$	
L_p (in.)	s_{pa}	s_{dpa}	s_{dpe}	s_{dpa}	s_{dpe}	s_{dpa}	s_{dpe}
0.5	10.5	11.6	11.7	104.1	105.1	219.5	222.0
3.0	3.7	4.7	4.8	42.0	43.0	88.5	90.7
4.0	3.0	4.0	4.0	35.2	36.1	74.1	76.3
5.0	2.5	3.5	3.5	30.3	31.3	63.7	66.0
6.0	2.1	3.0	3.0	26.4	27.4	55.5	57.9
7.0	1.8	2.7	2.7	23.2	24.3	48.6	51.3
8.0	1.5	2.4	2.4	20.3	21.6	42.3	45.5
9.0	1.3	2.1	2.1	17.4	19.1	36.1	40.3
9.3	1.2	1.9	2.0	14.5	17.6	29.8	37.1

The total steady-state potential drop, Δp_t, can be expressed in terms of individual potential drops in Regions 1 and 2:

$$\Delta p_t=\Delta p_2+\Delta p_1, \quad \text{(A-1)}$$

where Δp_2 can be trivially found from the solution of radial-flow equations and Δp_1 is a function of perforation parameters and the relative location of the damaged zone, r_d, with respect to perforations (boundary effect). Consequently, Δp_1 can be defined in terms of the perforation skin, s_p, and a pseudoskin, s_x, which takes into account any pressure gain resulting from the proximity of perforations to the damaged-zone boundary.

$$\frac{q_o\mu}{2\pi kh_t}\left(\ln\frac{r_e}{r_w}+s_t\right)=\frac{q_o\mu}{2\pi kh_t}\left(\ln\frac{r_e}{r_d}\right)+\frac{q_o\mu}{2\pi k_d h_t}\left(\ln\frac{r_d}{r_w}+s_p+s_x\right). \quad \text{(A-2)}$$

For unidirectional 0°-phased perforations, s_x can be approximated by Muskat's[15] off-centered-well solutions:

$$s_x \simeq \ln\left[1-\frac{1}{r_d^2}\left(r_w+\frac{L_p}{2}\right)^2\right]. \quad \text{(A-3)}$$

Table 5 illustrates the boundary effects for 180°-phased perforations obtained by 2D finite-element simulations for various external radii. The skin resulting from boundary effects, s_x, as inferred from Table 5, is not significant for $r_d \geq 1.5(r_w+L_p)$.

Rearranging Eq. A-2 and using Eq. 2 yields

$$s_{dp}=\left(\frac{k}{k_d}-1\right)\left[\ln\left(\frac{r_d}{r_w}\right)+s_p\right]+\frac{k}{k_d}s_x. \quad \text{(A-4)}$$

To demonstrate the validity of the formulation presented above, we compared the damage skin, s_{dp}, calculated from finite-element simulations with that obtained from Eqs. A-3 and A-4 for 0°-phased perforations. As **Table A-1** shows, three different k_d/k were assumed in these comparisons. The damaged-zone radius was fixed ($r_d=14$ in. [35.5 cm]) and the perforation length was successively increased. As depicted in Table A-1, the damage-skin estimates (obtained with Eq. A-4), s_{dpe}, compare quite well with the actual skin values, s_{dpa}, obtained by direct finite-element simulations. The perforation skin factor (shown as s_{pa} in Table A-1) is also obtained through finite-element simulations.

SI Metric Conversion Factors

ft × 3.048*	E−01	=	m
in. × 2.54*	E+00	=	cm

*Conversion factor is exact.

SPERE

Original SPE manuscript received for review Oct. 2, 1988. Paper accepted for publication April 30, 1990. Revised manuscript received April 11, 1990. Paper (SPE 18247) first presented at the 1988 SPE Annual Technical Conference and Exhibition held in Houston, Oct. 2–5.

SPE 21477, "Supplement to SPE 18247, Semianalytical Productivity Models for Perforated Completions," available from SPE Book Order Dept.